Chapter 18
Polymorphism of Hafnia-Based Ferroelectrics for Ferroelectric Field-Effect Transistors

Min Hyuk Park

Abstract In this chapter, the thermodynamic and kinetic origins of the unexpected ferroelectric phase formation in emerging fluorite-structure oxides such as HfO_2 and ZrO_2 are discussed. Various thermodynamic factors, such as doping, stress, and surface/interface/grain boundary energies, could affect the relative free energies of crystalline phases. However, several phenomena including the effects of annealing temperature could not be explained by thermodynamic factors. In this regard, a kinetic mechanism was recently suggested to understand the metastable ferroelectric phase formation. Previous studies on the mechanism of the ferroelectric phase formation are comprehensively critically reviewed to understand the unexpected ferroelectric phase formation.

The ferroelectricity in fluorite-structure oxides such as HfO_2 and ZrO_2, initially reported by Boescke et al. [1] in 2011, attracts increasing interest in terms of both industrial applications and fundamental science [2]. Unlike the conventional ferroelectric materials based on perovskite and layered perovskite structures, the fluorite-structure ferroelectrics can be scaled down even below a film thickness of 10 nm while maintaining the robust ferroelectric properties [1, 2]. Therefore, these new ferroelectric materials are considered very promising for the development of ferroelectric field-effect transistors (FeFETs) compatible with the complementary metal–oxide–semiconductor (CMOS) technology [1–4]. Moreover, the negative capacitance effect in ferroelectric fluorite-structure oxides is intensively studied to overcome the theoretical limit (60 meV/dec) of the subthreshold swing of MOSFETs [5–8].

For applications such as FeFETs, the control of the material properties strongly related to their crystalline phases is crucial to achieving uniform and reliable devices. In the phase diagrams of the bulk HfO_2 and ZrO_2, no ferroelectric phases can be observed at any pressure and temperature [9, 10]. However, ferroelectricity in HfO_2-based thin films could be reproducibly induced by various dopants and deposition

M. H. Park (✉)
School of Materials Science and Engineering, Pusan National University,
Busandaehak-ro-63-beon-gil 2, Busan 46241, South Korea
e-mail: minhyukpark@pusan.ac.kr

© Springer Nature Singapore Pte Ltd. 2020

B.-E. Park et al. (eds.), *Ferroelectric-Gate Field Effect Transistor Memories*,
Topics in Applied Physics 131, https://doi.org/10.1007/978-981-15-1212-4_18

techniques [2]. Boeske et al. [1] suggested that the noncentrosymmetric orthorhombic phase with a space group of $Pca2_1$ is the origin of the unexpected ferroelectric properties. Sang et al. [11] for the first time experimentally demonstrated that a ferroelectric Gd-doped HfO_2 film had the $Pca2_1$ orthorhombic crystalline structure, based on transmission electron microscopy and convergent electron beam diffraction. To understand the unexpected ferroelectric phase formation, numerous research groups studied the ferroelectric phase formation in HfO_2-based thin films based on thermodynamics and kinetics. In this chapter, studies on the thermodynamic and kinetic origins of the ferroelectric phase formation are reviewed.

18.1 Thermodynamic Stabilization of the *Pca2₁* Orthorhombic Phase

18.1.1 Effects of Dopants

Dopings of various cations or even anions such as N induced ferroelectricity in HfO_2 thin films [1, 2, 12–22]. The effects of cation and anion dopings on the relative free energies of various crystalline phases of HfO_2 have been studied. Boescke et al. [1] reported ferroelectricity in a 3.1%-Si-doped HfO_2 thin film while an antiferroelectric-like behavior was observed for a 4.3%-Si-doped film. Subsequently, the effects of the doping concentration on the electrical properties of doped HfO_2 thin films have been reported for various dopants including Si [1], Al [12], Gd [19], Zr [13–15], Y [16, 17], Sr [20], and La [21].

Schroeder et al. [22] reported the effects of the doping concentrations on the ferroelectric or antiferroelectric properties of HfO_2 thin films doped with various dopants. For all of the considered dopants, ferroelectric properties were observed in specific doping concentration ranges, which depended on the dopant species [22]. When the doping concentration was increased over the specific range, only the dopants smaller than Hf (Al and Si) and Zr could induce the antiferroelectric-like behavior [22]. However, the origin of the effect of the dopant size is not clearly understood yet. Park et al. [23] comprehensively studied the effects of the doping concentration and annealing conditions on the electrical and structural properties of doped HfO_2 thin films. They experimentally demonstrated that the ferroelectric orthorhombic phase fraction is affected by the doping concentration [23]. With the increase in the doping concentration, the dominant crystalline phase changes from the monoclinic to the tetragonal phase through the intermediate orthorhombic phase [23]. For a 10-nm-thick film, the maximum orthorhombic phase fraction was approximately 70–80% [23].

Starschich et al. [18, 24, 25] analyzed the effects of the doping concentration on the ferroelectric properties of chemical-solution-deposited (CSD) HfO_2 thin films and confirmed a trend similar to that of atomic-layer-deposited (ALD) films. The rather strong ferroelectricity could be induced in a specific concentration range by

doping cations such as Y, Sr, Ba, Er, Sm, Nd, and La, but for some dopants such as Al, Ga, Co, Ni, Mg, and In, the maximum achievable P_r values were quite small (smaller than 5 $\mu C/cm^2$) [24]. They reported that dopants whose ionic radii are larger than 85 pm could efficiently induce high fractions of the ferroelectric phase in HfO_2 thin films [24]. For some dopants such as Al, the ferroelectricities of ALD and CSD films were completely different, suggesting that the deposition technique can also affect the ferroelectric phase formation in HfO_2 thin films [24].

Xu et al. [26] studied the effects of the concentrations of various dopants, such as Sc, Y, Nb, Al, Si, Ge, Zr, and N, in physical-vapor-deposited HfO_2 thin films and observed that the changes in relative fractions of the crystalline phases were almost the same for all of the tested dopants [26]. Therefore, they suggested that they could observe a universal phase transition path by varying the doping concentrations [26]. Although the doping concentration range for the ferroelectric phase formation strongly depended on the dopant species, the experimental P_r–monoclinic-phase-fraction plot was consistent for all of the dopants [26].

Therefore, the experimental studies showed that doping is a key factor, which strongly influences the ferroelectric properties of HfO_2 thin films with various dopants obtained by various deposition techniques. The dopant species determine whether the ferroelectricity and antiferroelectricity can be achieved. Moreover, the dopant species affect the doping concentration range for the ferroelectricity or antiferroelectricity. With the increase in the doping concentration, the dominant crystalline phase changes from the monoclinic to the tetragonal or cubic phase through the intermediate ferroelectric orthorhombic phase.

On the other hand, extensive computer simulation studies related to this issue have been carried out. Huan et al. [27] analyzed the relative free energies of various crystalline phases including two polar orthorhombic phases (space groups: $Pca2_1$ and $Pmn2_1$) of the bulk HfO_2. They showed that the free energy differences between the two polar orthorhombic phases and stable monoclinic phase are rather small at high pressure [27]. Reyes-Lillo et al. [28] studied the free energy barriers between the $Pca2_1$ orthorhombic and $P4_2/nmc$ tetragonal phases as well as the free energies of various crystalline phases. They showed that owing to the small energy difference between the tetragonal and $Pca2_1$ orthorhombic phases, a field-induced phase transition and resulting antiferroelectric-like behavior were expected for ZrO_2 [28]. In these two studies, published in 2014, for the first time, the free energies of various crystalline phases in HfO_2 and ZrO_2 were analyzed; however, the effect of doping was not considered.

Materlik et al. [29] reported the relative free energies of various crystalline phases of the HfO_2–ZrO_2 solid solution system with various Zr/(Hf + Zr) ratios. They showed that with the increase in the Zr/(Hf + Zr) fraction, the free energy differences between the metastable phases, such as the $Pca2_1$ orthorhombic and $P4_2/nmc$ tetragonal phases, and stable monoclinic phase decrease [29]. However, the effect of doping was not sufficient to stabilize the metastable orthorhombic or tetragonal phase, as the free energy difference was too large to be overcome solely by doping [29]. Therefore, they considered the surface energy effect, which is generally attributed to the stabilization mechanism of the metastable tetragonal phase in ZrO_2 thin films

[29]. However, they did not calculate the surface energy by computer simulation. Instead, they estimated the surface energy of the ferroelectric orthorhombic phase to understand the experimentally observed ferroelectric phase formation between the tetragonal and monoclinic phases by varying the Zr content and thickness of the $Hf_{1-x}Zr_xO_2$ film [29].

Batra et al. [30] analyzed the effects of various factors including doping, stress, electric field, and surface energy on the polymorphism of HfO_2 thin films. They concluded that the ferroelectric phase cannot be stabilized by a single factor, but can be thermodynamically stabilized by contributions of various factors [30]. Batra et al. [31] comprehensively analyzed the effect of doping by investigating numerous dopants of the periodic table. They analyzed the effects of 3.125% dopings on the free energies of crystalline phases for numerous dopants and selected dopants that could induce large decreases in free energy differences between the orthorhombic and monoclinic phases. Subsequently, the additional effect of oxygen vacancies doped along with the dopant for charge neutrality was considered. Six dopants, Ca, Sr, Ba, La, Y, and Gd, had the strongest effects on the stabilization of the ferroelectric orthorhombic phase [31]. However, even with these dopants, the ferroelectric orthorhombic phase could not be thermodynamically stabilized [31].

Therefore, the doping can decrease the free energy difference between the ferroelectric orthorhombic and monoclinic phases, according to the computer simulations, but the ferroelectric orthorhombic phase could not be thermodynamically stabilized only by the doping. Other thermodynamic factors or even kinetic mechanisms should be considered to understand the ferroelectric phase formation in HfO_2-based thin films.

18.1.2 Surface/Interface/Grain Boundary Energy Effects

According to experiments, the ferroelectric properties of HfO_2-based thin films degrade with the increase in the film thickness [15, 32]. Park et al. [15] showed that the monoclinic phase fraction in a $Hf_{0.5}Zr_{0.5}O_2$ thin film increases with the film thickness. Yurchuk et al. [32] also reported that the monoclinic phase fraction in a Si-doped HfO_2 thin film increases with the film thickness. A similar trend was experimentally confirmed in many other studies although the critical thicknesses for the monoclinic phase formation slightly differed. Kim et al. [33] and Riedel et al. [34] showed that by periodically inserting Al_2O_3 interlayers at every 10 nm of $Hf_{0.5}Zr_{0.5}O_2$, the monoclinic phase fraction could be significantly reduced with a decreased average grain size as the continuous growth of grains could be prohibited by the Al_2O_3 interlayers.

Materlik et al. [29] suggested that the ferroelectric phase in a $Hf_{0.5}Zr_{0.5}O_2$ thin film can be stabilized by the surface energy effect. It is well known that for ZrO_2 thin films, the metastable tetragonal phase can be stabilized by the surface energy effect, as the surface energy of the tetragonal phase is significantly lower than that of the

monoclinic phase [35–37]. According to experimental observations of ferroelectric-doped HfO_2 and HfO_2–ZrO_2 solid solution, the ferroelectric phase can be formed in the thickness range between those of the tetragonal and monoclinic phases [15, 38]. Therefore, Materlik et al. [29] suggested that the bulk and surface free energies of the orthorhombic phase would be between those of the tetragonal and monoclinic phases. Consequently, the ferroelectric phase can be formed in a specific thickness range between those for the tetragonal and monoclinic phases [29]. However, they did not directly calculate the surface free energies of the crystalline phases. Instead, they estimated the surface free energy, which could explain the experimental observations [29]. Künneth et al. [39] suggested that the grain boundaries of a doped HfO_2 film might have the tetragonal structure and estimated the grain boundary free energy by the interface energies between the bulk crystalline (monoclinic, orthorhombic, and tetragonal) and tetragonal phases. However, in polycrystalline-doped HfO_2 films, the grains have independent orientations, and thus additional grain boundaries exist between the outer tetragonal shells of adjacent grains. Moreover, core–shell structure of grains was not experimentally demonstrated while the tetragonal phase at a doped HfO_2/electrode interface was reported [40, 41].

Batra et al. [42] calculated the surface free energies of various crystalline phases of HfO_2 with various orientations. For almost all orientations, the surface free energy of the $Pca2_1$ orthorhombic phase was higher than that of the monoclinic phase. Therefore, the stabilization of the orthorhombic phase could not be explained by the surface energy effect [42]. They considered two potential ferroelectric orthorhombic phases; the results suggested that only the $Pmn2_1$ orthorhombic phase could be stabilized by the surface energy effect [42]. However, the X-ray diffraction (XRD) pattern of the $Pmn2_1$ orthorhombic phase is quite different from the experimentally observed pattern, and thus the $Pca2_1$ orthorhombic phase formation could not be understood by considering the surface energy effect.

In computer simulations, generally, the surface free energies have been considered to understand the experimentally observed size effect. However, it should be noted that polycrystalline samples generally do not have free surfaces. Instead, only interfaces between the doped HfO_2 film and electrodes and grain boundaries exist. It is generally known that the high-angle grain boundary energy is approximately 1/3 of the surface free energy and that the interfacial energy should be significantly lower than the surface free energy. Therefore, the effects of the interface and grain boundary energies are expected to be significantly smaller than the calculated effect of the free surface. It should be also noted that the calculation of the surface free energy is very challenging for compounds with more than two ions or atoms. The surface free energy is strongly affected by surface chemical species, orientations, and relaxation of lattices. Therefore, it is believed that the experimentally observed size effect could not be clearly understood based on computational simulations.

18.1.3 Effects of the Film Stress and Upper Capping Layer

The stress has been considered as another key factor for the formation of the ferroelectric phase in doped HfO_2 thin films. In their study on the ferroelectricity of a Si-doped HfO_2, Boescke et al. [1] showed that the TiN upper capping layer could hinder the formation of the stable monoclinic phase and suggested that this effect might be related to the stress from the TiN capping layer. Park et al. suggested that in-plane tensile stress would have a positive effect on the formation of the orthorhombic phase considering its lattice parameters [43]. In the orthorhombic HfO_2 or ZrO_2, the *a*-axis parameter is larger than the *b*- and *c*-axis (polar axis) parameters by ~3.5–4% [29]. Subsequently, Park et al. reported that a (111)-oriented $Hf_{0.5}Zr_{0.5}O_2$ film deposited on a Pt electrode could not exhibit ferroelectricity and suggested that the almost equivalent stresses in the *a*-, *b*-, and *c*-axes of the (111)-oriented film might be the origin for the absence of ferroelectricity [43]. They also suggested that anisotropic stress would be favorable for the ferroelectric phase formation [43].

Schenk measured the stress in a 10-nm-thick Si-doped HfO_2 thin film using the $\sin^2\Psi$ method by XRD and reported tensile stress even higher than 2 GPa [44]. Schroeder et al. [21] reported similar tensile stress in a La-doped HfO_2 thin film. Shiraishi et al. [45] studied the effects of the stress originating from the difference in thermal expansion coefficient between the HfO_2 film and substrate on the ferroelectric properties of a $Hf_{0.5}Zr_{0.5}O_2$ thin film [45]. They experimentally demonstrated that the remanent polarization increased with the tensile stress by decreasing the relative fraction of the monoclinic phase [45]. Kim et al. [46] evaluated the effect of the thickness of an upper TiN capping layer on the ferroelectric properties of a $Hf_{0.5}Zr_{0.5}O_2$ thin film. They reported that the film stress and P_r increased with the thickness of the upper TiN layer and concluded that the ferroelectric properties of the $Hf_{0.5}Zr_{0.5}O_2$ thin film were enhanced with the increase in the tensile stress [46].

Further, theoretical studies have been carried out on the effect of the film stress on the formation of the $Pca2_1$ orthorhombic phase. In 1999, Lowther et al. [47] analyzed the effects of hydrostatic pressure on the free energies of various crystalline phases of ZrO_2 and HfO_2. The free energies of the *Pbca* orthorhombic phase (high-pressure phase of HfO_2 and ZrO_2) and the $Pca2_1$ orthorhombic phase were very similar; the difference was smaller than 10 meV/f.u. [48]. For some regions of the unit cell, the free energy of the $Pca2_1$ orthorhombic phase was even lower than that of the *Pbca* phase [48]. However, the hydrostatic pressure condition considered in their study is quite different from the biaxial stress condition in thin films. Reyes-Lillo et al. [28] analyzed the effects of epitaxial stress on the relative free energies of various crystalline phases such as the cubic, tetragonal, $Pca2_1$ orthorhombic, and monoclinic phases of ZrO_2. They considered in-plane biaxial stress for an *a*-axis-oriented $Pca2_1$ orthorhombic phase [28]. It should be noted that the *a*-axis is the longest (i.e., its parameter) nonpolar axis, and thus the polar *c*-axis is oriented in-plane. This is different from the configurations in ferroelectric-doped HfO_2 films with substrate-normal polarizations, which is useful for memory applications. In

this in-plane polarization geometry, an epitaxial compressive strain larger than -0.01 could stabilize the ferroelectric orthorhombic phase.

In 2015, Materlik et al. [29] comprehensively analyzed the effects of stress on the free energies of various polymorphs of HfO_2, $Hf_{0.5}Zr_{0.5}O_2$, and ZrO_2. They reported that the strain-induced *f*-phase is stable only for a compressive strain applied in the *ac*-plane of the orthorhombic phase [29]. As the *c*-axis of the orthorhombic phase is the polar axis, this orientation is not suitable to understand the film stress effect in HfO_2 films with substrate-normal polarizations. Therefore, they also analyzed the biaxial stress in the (110) plane. The $Pca2_1$ orthorhombic phase can be stabilized under a compressive stress of 7–8 GPa, which is believed to be unreasonably high. Therefore, they concluded that the orthorhombic phase cannot be stabilized solely by stress. Batra et al. [30] analyzed the effects of both hydrostatic and equibiaxial stresses on the free energies of various crystalline phases of HfO_2. The free energy of the $Pca2_1$ orthorhombic phase was lower when a sufficient compressive biaxial stress was applied [30]. However, even in this case, the *Pbca* orthorhombic phase could have free energy lower than that of the $Pca2_1$ orthorhombic phase [30].

In summary, in the experiments, large in-plane tensile stresses at the few-gigapascal level were generally observed for ALD films, while according to the theory, the effect of the compressive biaxial stress could decrease the free energy of the ferroelectric orthorhombic phase. According to the theoretical calculations, the ferroelectric phase stabilized by compressive stress has an in-plane polarization, which is not consistent with the experimental observations. Therefore, the $Pca2_1$ orthorhombic phase stabilization cannot be explained by the effect of the film stress. Instead, the free energy difference between the ferroelectric orthorhombic and tetragonal phases can be overcome by the stress effect, as shown by several theoretical studies.

18.2 Kinetic Mechanism

Park et al. [38] comprehensively compared the experimental results of the HfO_2–ZrO_2 solid solution system for various thicknesses and compositions to the surface energy model suggested by Materlik et al. [29]. As samples generally have interfaces and grain boundaries instead of free surfaces, they assumed that the interface and grain boundary energies are ~1/3 of the surface free energy [38]. With this assumption, the observed thickness and composition ranges for the ferroelectric properties could not be well understood. To stabilize the ferroelectric phase, a higher Zr concentration and smaller thickness were required.

On the other hand, when the interface/grain boundary energy model was applied to the nanocrystallites with an average radius of 2 nm, which existed in the as-deposited film, the expected crystalline phase was consistent with the final crystalline phase in the fully crystalline state [38]. Based on this result, Park et al. [38] concluded that the crystalline phase of the $Hf_{0.5}Zr_{0.5}O_2$ film is already determined during the

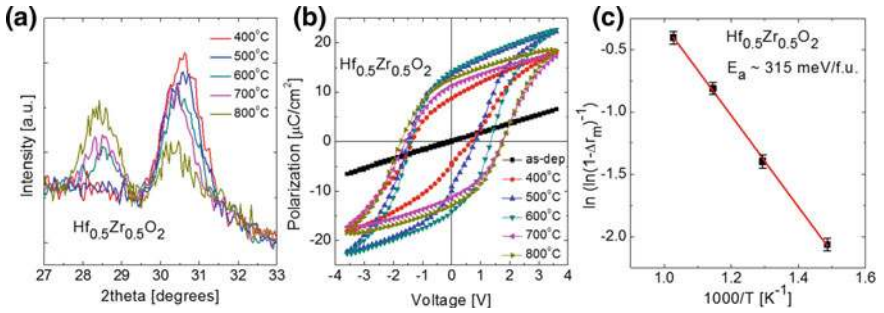

Fig. 18.1 **a** GIXRD results and **b** polarization–electric-field (P–E) curves of 9.2-nm-thick $Hf_{0.5}Zr_{0.5}O_2$ films. **c** Arrhenius plot of the increase in monoclinic phase fraction (Δr_m) against 1000/T based on the JMA model. The error bars show the areal errors from the Gaussian fittings for the GIXRD patterns. Adapted from Ref. [48] with permission. Copyright 2018, Royal Society of Chemistry

nucleation process and that the phase transition to the stable monoclinic phase might be kinetically suppressed.

Subsequently, Park et al. revisited the effects of annealing temperature on the ferroelectric properties of $Hf_{0.5}Zr_{0.5}O_2$ thin films [48]. According to thermodynamic models, in principle, the annealing temperature is not expected to affect the final crystalline phase, unless the thermodynamic factors such as the grain size do not vary with the annealing temperature. However, the ferroelectric properties were strongly affected by the annealing temperature. Figures 18.1a and b show grazing-incidence X-ray diffraction (GIXRD) patterns and polarization–electric-field curves of $Hf_{0.5}Zr_{0.5}O_2$ thin films annealed at various temperatures in the range of 400–800 °C. With the increase in the annealing temperature, the monoclinic phase fraction significantly increases, as shown in Fig. 18.1a; the changes in P_r are consistent with the changes in relative fractions of the crystalline phases. They analyzed the change in the grain size of the $Hf_{0.5}Zr_{0.5}O_2$ thin film with the annealing temperature; almost no changes were observed [48]. The possibility of a frozen high-temperature phase was also considered. With this model, when the sample is annealed at a higher temperature, a higher fraction of the high-temperature phase might exist even after cooling. Therefore, based on the frozen phase model, the tetragonal/orthorhombic phase fraction is expected to increase with the annealing temperature, which is opposite to the experimental observation [48]. To explain the effect of the annealing temperature, Park et al. assumed that the ferroelectric phase fraction is governed by the kinetic suppression of the formation of the stable monoclinic phase [48]. They reported an Arrhenius-type plot based on the well-known Johnson–Mehl–Avrami (JMA) model for the phase transition from the tetragonal/orthorhombic to the monoclinic phase showing a clear linear relation, which well fitted the kinetic model [48]. The activation energy barrier estimated by the Arrhenius plot was ~315 meV/f.u., which well matches with the value estimated based on the elastic deformation required for

the phase transition from the metastable tetragonal phase to the monoclinic phase (~250 meV/f.u.) [48].

Park et al. [49] comprehensively reviewed their sample fabrication process for a detailed understanding of the ferroelectric phase formation in a $Hf_{0.5}Zr_{0.5}O_2$ thin film. Figure 18.2a shows a schematic phase diagram of $Hf_{0.5}Zr_{0.5}O_2$ thin films. Figures 18.2b, d, f, h, and j show schematics of the $Hf_{0.5}Zr_{0.5}O_2$ films while Figs. 18.2c, e, g, i, and k show schematic free energy curves of the tetragonal, orthorhombic, and monoclinic phases in various steps of the sample fabrication. The $Hf_{0.5}Zr_{0.5}O_2$ thin film was deposited by thermal ALD at 280 °C. The deposited $Hf_{0.5}Zr_{0.5}O_2$ thin film was taken out from the ALD chamber to the atmosphere. As shown in Fig. 18.2b, nanocrystallites with an average diameter of 4 nm were formed during the deposition. The average nanocrystallite size was estimated by the Scherrer equation using the width of the (111) orthorhombic/tetragonal XRD peak. Figure 18.2c shows schematic free energy curves obtained using the free energies of the tetragonal, orthorhombic, and monoclinic phases considering the interface/grain boundary energy effect and bulk free energies reported by Materlik et al. [29]. As shown in Fig. 18.2c, the orthorhombic phase had the lowest free energy among those of the three crystalline phases considered in the study.

The partially crystalline as-deposited films were annealed by a rapid thermal process (RTP) at 400–600 °C for 30 s in an N_2 atmosphere. After the rapid ramping, the temperature reached 600 °C; the changes in grain size were negligible owing to the short period of ramping, as shown in Fig. 18.2d. As shown in Fig. 18.2e, the stable crystalline phase might change to the tetragonal phase, as the entropy of the tetragonal phase is higher than those of the orthorhombic and monoclinic phases. Subsequently, crystallization of the whole $Hf_{0.5}Zr_{0.5}O_2$ thin film occurs with a rapid grain growth, as shown in Fig. 18.2f. Owing to the increase in the grain size, the stable phase of the final grains changed to the monoclinic phase, as shown in Fig. 18.2g. However, as discussed above, the activation energy barrier for the transition from the tetragonal to the monoclinic phase is even higher than 250 meV/f.u. so that the phase transition to the monoclinic phase is prevented. Consequently, the $Hf_{0.5}Zr_{0.5}O_2$ thin film can exist in the second stable tetragonal phase. However, when the annealing temperature or time at a high temperature increases, the high free energy barrier might be also overcome by sufficient thermal energy. Therefore, the control of the annealing temperature and time is important to induce the ferroelectric phase in $Hf_{0.5}Zr_{0.5}O_2$ or doped HfO_2 thin films.

After the high-temperature process, the sample was cooled down to room temperature (RT) in the RTP chamber, and, as shown in Figs. 18.2h, and i, the second stable phase changes from the tetragonal to the orthorhombic phase. The phase transition from the tetragonal to the orthorhombic phase might easily occur owing to their rather low kinetic energy barrier. Based on the elastic energy estimated by the differences in lattice parameters and elastic coefficients, the energy barrier was even lower than 30 meV/f.u., which is similar to the kT value at RT (~25 meV/f.u.). Finally, at RT, the ferroelectric orthorhombic phase can be formed in polycrystalline $Hf_{0.5}Zr_{0.5}O_2$ thin films. Park et al. [49] suggested that the metastable ferroelectric phase can be formed even when this phase is not thermodynamically stabilized.

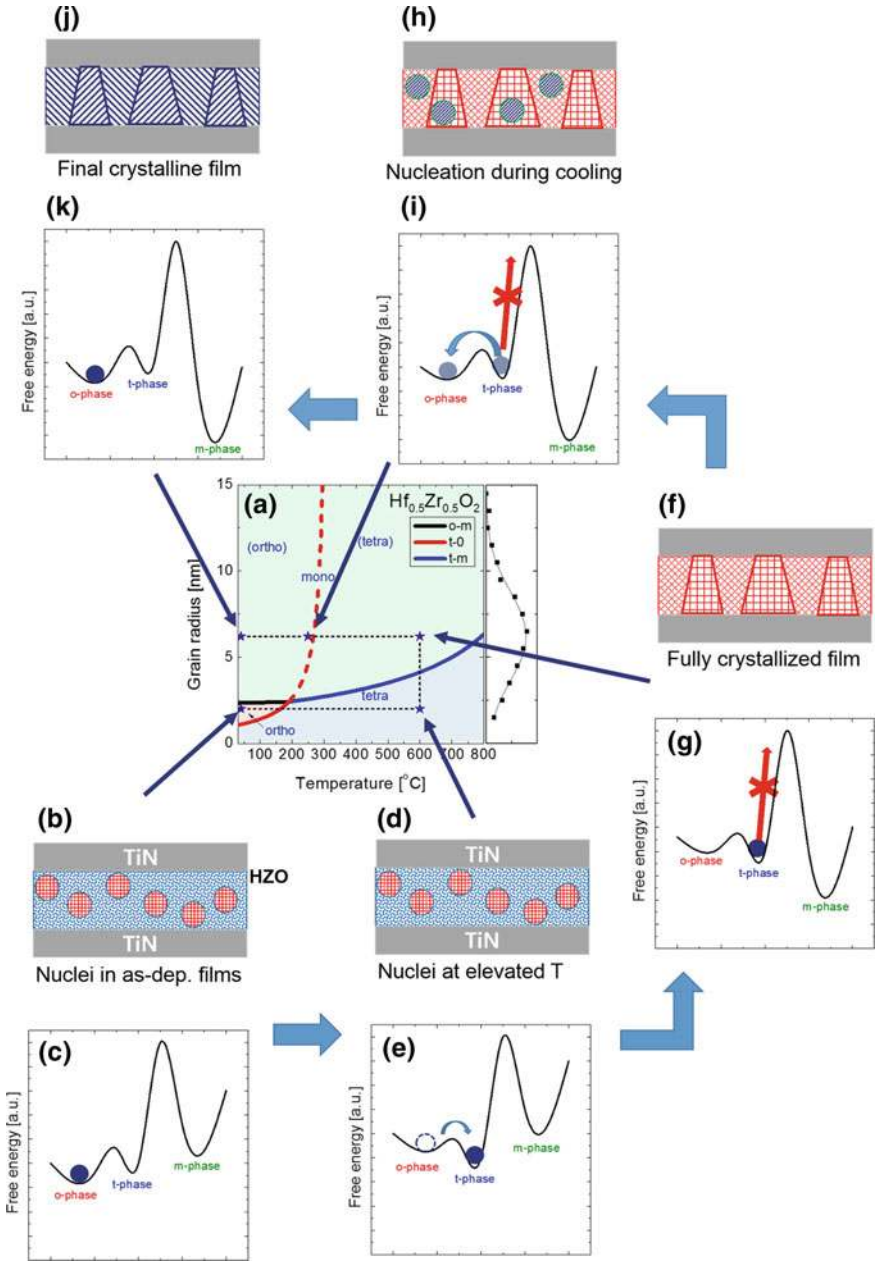

Fig. 18.2 **a** Schematic phase diagram for the 9.2-nm-thick $Hf_{0.5}Zr_{0.5}O_2$ thin films with various grain radii at various temperatures. **b**, **d**, **f**, **h**, **j** Schematics and **c**, **e**, **g**, **i**, **k** free energy curves of crystallites, illustrating the films before and during the RTP for the film crystallization. Reproduced from Ref. [49] with permission. Copyright 2019 John Wiley and Sons

Park et al. [50] analyzed the crystallization process of ferroelectric-doped HfO_2 thin films using in situ XRD. They evaluated four different dopants, Al, Gd, Sr, and Si, with concentrations optimized to provide the largest P_r values. It is worth noting that very similar trends were observed for the four tested dopants. Figure 18.3a shows the in situ XRD patterns measured in the range of RT to 1000 °C. In the as-deposited state, the doped HfO_2 film exists in the amorphous state, while above 500 °C, it crystallizes into the tetragonal phase, as shown in Fig. 18.3a. With the further increase in the

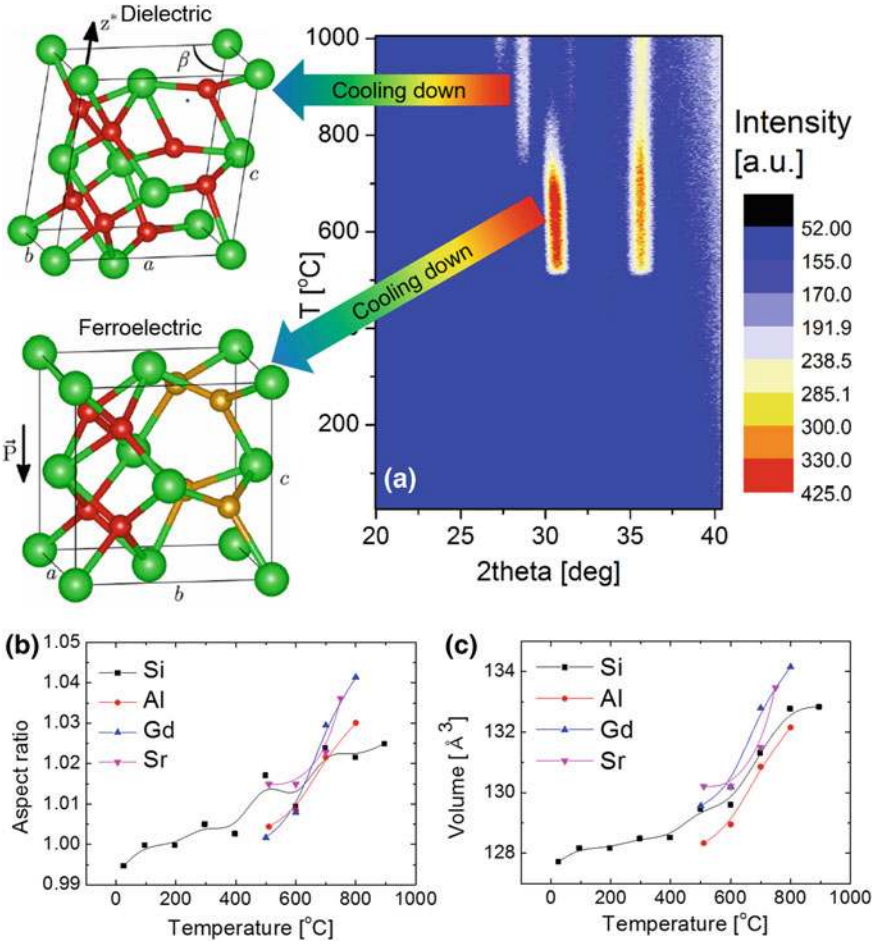

Fig. 18.3 **a** In situ high-temperature XRD results in the range of RT to 1000 °C, interpreted as a colored contour map with the crystalline structures of the monoclinic (left upper panel) and ferroelectric orthorhombic (left middle panel) phases. Changes in the **b** aspect ratios of $2a/(b + c)$ for the orthorhombic phase and c/a for the tetragonal phase and **c** unit cell volume calculated using the diffraction peak locations in the in situ XRD patterns. Reproduced from Ref. [49] with permission. Copyright 2019 John Wiley and Sons

temperature above ~600 °C, the (011)t diffraction peak at 2θ of 30.5° shifted to a lower 2θ suggesting that the interplanar distance increased. However, the shift of the (110)t diffraction peak was negligible, which implies changes in the aspect ratio, i.e., the relative ratio of the longest axis to the two shorter axes. Park et al. [51] suggested that this parameter is useful to distinguish the ferroelectric orthorhombic phase from the tetragonal phase. With the further increase in the temperature even above 800 °C, the stable monoclinic phase was formed, as shown in Fig. 18.3a. The changes in the aspect ratio (Fig. 18.3b) and unit cell volume (Fig. 18.3c) were also analyzed using the in situ XRD patterns. The aspect ratio, i.e., the relative ratio of the longest axis to the two shorter axes, is $2a/(b + c)$ for the orthorhombic phase and c/a for the tetragonal phase (when a double-size unit cell with 4 Hf ions and 8 oxygen ions is considered). It should be noted that the aspect ratio of the orthorhombic phase is ~1.03–1.04 while that of the tetragonal phase is expected to be ~1.02, and that the unit cell volume of the orthorhombic phase is larger than that of the tetragonal phase by ~2% [50]. Therefore, the changes in the aspect ratio and unit cell volume with the increase in the temperature also support the result that the dominant crystalline phase changes from the tetragonal phase to the orthorhombic phase with the increase in the temperature before reaching the temperature for the monoclinic phase formation.

The in situ XRD results suggest that the ferroelectric phase might not be thermodynamically stabilized, as, at a high temperature, the stable monoclinic phase was formed in the doped HfO_2 thin film. It should be noted that the metastable tetragonal and orthorhombic phases have higher entropies than that of the monoclinic phase. The doped HfO_2 thin film initially crystallized into the metastable tetragonal phase. Before the formation of the stable monoclinic phase, the intermediate orthorhombic phase was formed. This process is reasonable in terms of structure as the orthorhombic phase has intermediate properties between those of the tetragonal and monoclinic phases. In a previous study, the $Pca2_1$ orthorhombic phase was suggested as an intermediate state between the tetragonal and monoclinic phases [51].

In 2018, Lee et al. [52] carried out a comprehensive experiment to investigate the mechanism of the transition from the tetragonal/orthorhombic phase to the monoclinic phase. They fabricated ferroelectric $Hf_{0.5}Zr_{0.5}O_2$ thin films sandwiched by top and bottom TiN electrodes [52]. The films crystallized mostly into the orthorhombic phase during the rapid thermal process [52]. Subsequently, in half of the samples, the upper TiN electrode was removed while the other samples still had TiN upper capping layers. The ferroelectric $Hf_{0.5}Zr_{0.5}O_2$ thin films with and without the TiN upper capping layer were annealed at various temperatures (400–600 °C) for various times (1–10^4 s) [52]. The monoclinic phase fractions in the annealed films were then analyzed to investigate the mechanism of the monoclinic phase formation [52]. They assumed a phase transition according to the JMA model. However, the growth dimension exponent was in the range of 0.2–0.4, which implies that the phase transition should be affected by other factors [52]. Therefore, they applied a nucleation-limited phase transition model based on a nucleation-limited switching model for the kinetic mechanism for polarization switching in ferroelectric materials. In this model, it is assumed that the initiation point for nucleation has a statistical distribution different

from that of the JMA model with the initiation of the crystallization at the same time. Consequently, the transition from the tetragonal/orthorhombic to the monoclinic phase could be well explained by the rather high kinetic energy barriers of 1.67 and 2.14 eV/f.u. for the samples without and with the TiN upper layer, respectively [52]. Therefore, they suggested that the TiN upper layer increased the kinetic barrier for the monoclinic phase formation by suppressing the surface diffusion of ions or stress effect [52].

18.3 Conclusion

In this chapter, the thermodynamic and kinetic mechanisms of the unexpected ferroelectric orthorhombic phase formation in fluorite-structure oxide thin films were reviewed. In terms of thermodynamics, various factors such as doping, surface/interface/grain boundary energies, and film stress affect the polymorphism of doped HfO_2 thin films. However, according to the theoretical studies based on computer simulations, the stabilization of the ferroelectric orthorhombic phase could not be quantitatively explained although it is certain that the free energy difference between the orthorhombic and monoclinic phases can be decreased by these factors. Moreover, the effect of the annealing temperature on the relative fraction of the stable monoclinic phase could not be understood based on thermodynamics.

Therefore, the kinetic mechanism was based on the assumption that the thermodynamically stable crystalline phase is the monoclinic phase even considering the effects of various thermodynamic factors such as doping, film stress, and surface/interface/grain boundary energy. According to the kinetic model, the transition from the tetragonal/orthorhombic to the monoclinic phase can be suppressed owing to the rather high kinetic barrier between these phases. Based on the in situ XRD analysis of the crystallization of doped HfO_2 thin films, a two-step transition from the tetragonal to the stable monoclinic phase with an intermediate ferroelectric orthorhombic phase could be observed, supporting the above kinetic mechanism.

Considering the current understanding of the ferroelectric phase formation in doped HfO_2 thin films, the film fabrication and crystallization annealing process must be adequately controlled. According to the kinetic mechanism, the thermodynamically stable phase is the monoclinic phase, which implies a driving force for the monoclinic phase formation when the ferroelectric phase is formed in doped HfO_2 thin films. However, there are still issues that are not clearly understood. Therefore, this field requires further studies to control the ferroelectric properties of HfO_2 thin films for FeFET applications.

Acknowledgements This research was supported by the Basic Science Research Program through the National Research Foundation (NRF) of Korea, grant-funded by the Ministry of Education (NRF-2018R1C1B5086580) and by the Global Frontier Program through the Global Frontier Hybrid Interface Materials of the NRF of Korea funded by the Ministry of Science and ICT (2013M3A6B1078874).

References

1. T.S. Böscke, J. Müller, D. Bräuhaus, U. Schröder, U. Böttger, Appl. Phys. Lett. **99**, 102903 (2011)
2. M.H. Park, Y.H. Lee, H.J. Kim, Y.J. Kim, T. Moon, K.D. Kim, J. Müller, A. Kersch, U. Schroeder, T. Mikolajick, C.S. Hwang, Adv. Mater. **27**, 1811 (2015)
3. T. Mikolajick, S. Slesazeck, M.H. Park, U. Schroeder, MRS Bull. **43**, 340 (2018)
4. M.H. Park, Y.H. Lee, T. Mikolajick, U. Schroeder, C.S. Hwang, MRS Commun. **8**, 795 (2018)
5. M. Hoffmann, M. Pešić, K. Chatterjee, A. I. Khan, S. Salahuddin, S. Slesazeck, U. Schroeder, T. Mikolajick, Adv. Funct. Mater. **26**, 8643 (2016)
6. M. Hoffmann, F.P.G. Fengler, M. Herzig, T. Mittmann, B. Max, U. Schroeder, R. Negrea, P. Lucian, S. Slesazeck, T. Mikolajick, Nature **565**, 464 (2019)
7. K.D. Kim, Y.J. Kim, M.H. Park, H.W. Park, Y.J. Kwon, Y.B. Lee, H.J. Kim, T. Moon, Y.H. Lee, S.D. Hyun, B.S. Kim, C.S. Hwang, Adv. Funct. Mater. 1808228 (2019) https://doi.org/10.1002/adfm.201808228
8. M. Si, C.-J. Su, C. Jiang, N.J. Conrad, H. Zhou, K.D. Maize, G. Qiu, C.-T. Wu, A. Shakouri, M.A. Alam, P.D. Ye, Nat. Nanotechnol. **13**, 24 (2018)
9. O. Ohtaka, H. Fukui, T. Kunisada, T. Fujisawa, K. Funakoshi, W. Utsumi, T. Irifune, K. Kuroda, T. Kikegawa, J. Am. Ceram. Soc. **84**, 1369 (2001)
10. O. Ohtaka, H. Fukui, T. Kunisada, T. Fujisawa, K. Funakoshi, W. Utsumi, T. Irifune, K. Kuroda, T. Kikegawa, Phys. Rev. B **63**, 174108 (2001)
11. X. Sang, E.D. Grimley, T. Schenk, U. Schröder, J.M. LeBeau, Appl. Phys. Lett. **106**, 162905 (2015)
12. S. Mueller, J. Mueller, A. Singh, S. Riedel, J. Sundqvist, U. Schroeder, T. Mikolajick, Adv. Funct. Mater. **22**, 2412 (2012)
13. J. Müller, T.S. Böscke, U. Schröder, S. Mueller, D. Bräuhaus, U. Böttger, L. Frey, T. Mikolajick, Nano Lett. **12**, 4318 (2012)
14. M.H. Park, H.J. Kim, Y.J. Kim, W. Lee, H.K. Kim, C.S. Hwang, Appl. Phys. Lett. **102**, 112914 (2013)
15. M.H. Park, H.J. Kim, Y.J. Kim, W. Lee, T. Moon, C.S. Hwang, Appl. Phys. Lett. **102**, 242905 (2013)
16. J. Müller, U. Schröder, T.S. Böscke, I. Müller, U. Böttger, L. Wilde, J. Sundqvist, M. Lemberger, P. Kücher, T. Mikolajick, L. Frey, J. Appl. Phys. **110**, 114113 (2011)
17. T. Olsen, U. Schröder, S. Müller, A. Krause, D. Martin, A. Singh, J. Müller, M. Geidel, T. Mikolajick, Appl. Phys. Lett. **101**, 082905 (2012)
18. S. Starschich, D. Griesche, T. Schneller, R. Waser, U. Böttger, Appl. Phys. Lett. **104**, 202903 (2014)
19. S. Mueller, C. Adelmann, A. Singh, S. V. Elshocht, U. Schroeder, T. Mikolajick, ECS J. Solid St. Sci. **1**, N123 (2012)
20. T. Schenk, S. Mueller, U. Schroeder, R. Materlik, A. Kersch, M. Popovici, C. Adelmann, S.V. Elshocht, T. Mikolajick, in *Proceedings of the European Solid-State Device Research Conference* (2013), p. 260.
21. U. Schroeder, C. Richter, M.H. Park, T. Schenk, M. Pešić, M. Hoffmann, F.P.G. Fengler, D. Pohl, B. Rellinghaus, C. Zhou, C.C. Chung, J.L. Jones, T. Mikolajick, Inorg. Chem. **57**, 2752 (2018)
22. U. Schroeder, E. Yurchuk, J. Müller, D. Martin, T. Schenk, P. Polakowski, C. Adelmann, M.I. Popovici, S.V. Kalinin, T. Mikolajick, Jpn. J. Appl. Phys. **53**, 08LE02 (2014)
23. M.H. Park, T. Schenk, C.M. Fancher, E.D. Grimley, C. Zhou, C. Richter, J.M. LeBeau, J.L. Jones, T. Mikolajick, U. Schroeder, J. Mater. Chem. C 5, 4677 (2017)
24. S. Starschich, U. Boettger, J. Mater. Chem. C 5, 333 (2017)
25. S. Starschich, T. Schenk, U. Schroeder, U. Boettger, Appl. Phys. Lett. **110**, 18 (2017)
26. L. Xu, T. Nishimura, S. Shibayama, T. Yajima, S. Migita, A. Toriumi, J. Appl. Phys. **122**, 124104 (2017)

27. T.D. Huan, V. Sharma, G.A. Rossetti Jr., R. Ramprasad, Phys. Rev. B **90**, 064111 (2014)
28. S.E. Reyes-Lillo, K.F. Garrity, K.M. Rabe, Phys. Rev. B **90**, 140103 (2014)
29. R. Materlik, C. Künneth, A. Kersch, J. Appl. Phys. **117**, 134109 (2015)
30. R. Batra, T.D. Huan, J.L. Jones, G. Rossetti Jr. R. Ramprasad, J. Phys. Chem. C **121**, 4139 (2017)
31. R. Batra, T.D. Huan, G.A. Rossetti Jr. R. Ramprasad, Chem. Mater. **29**, 9102 (2017)
32. E. Yurchuk, J. Müller, S. Knebel, J. Sundqvist, A.P. Graham, T. Melde, U. Schröder, T. Mikolajick, Thin Solid Films **533**, 88 (2013)
33. H.J. Kim, M.H. Park, Y.J. Kim, Y.H. Lee, W. Jeon, T. Gwon, T. Moon, K.D. Kim, C.S. Hwang, Appl. Phys. Lett. **105**, 192903 (2014)
34. S. Riedel, P. Polakowski, J. Mueller, AIP Adv. **6**, 095123 (2016)
35. R.C. Garvie, J. Phys. Chem. **69**, 1238 (1965)
36. R.C. Garvie, J. Phys. Chem. **82**, 218 (1978)
37. M.W. Pitcher, S.V. Ushakov, A. Navrotsky, B.F. Woodfield, G. Li, J. Boerio-Goates, J. Am. Ceram. Soc. **88**, 160 (2005)
38. M.H. Park, Y.H. Lee, H.J. Kim, T. Schenk, W. Lee, K.D. Kim, F.P.G. Fengler, T. Mikolajick, U. Schroeder, C.S. Hwang, Nanoscale **9**, 9973 (2017)
39. C. Künneth, R. Materlik, A. Kersch, J. Appl. Phys. **121**, 205304 (2017)
40. M. Pešić, F.P.G. Fengler, L. Larcher, A. Padovani, T. Schenk, E.D. Grimley, X. Sang, J.M. LeBeau, S. Slesazeck, U. Schroeder, T. Mikolajick, Adv. Funct. Mater. **26**, 4601 (2016)
41. E.D. Grimley, T. Schenk, T. Mikolajick, U. Schroeder, J.M. LeBeau, Adv. Mater. Interfaces **5**, 1701258 (2018)
42. R. Batra, H.D. Tran, R. Ramprasad, Appl. Phys. Lett. **108**, 172902 (2016)
43. M.H. Park, H.J. Kim, Y.J. Kim, T. Moon, C.S. Hwang, Appl. Phys. Lett. **104**, 072901 (2014)
44. T. Schenk, PhD thesis, TU Dresden
45. T. Shiraishi, K. Katayama, T. Yokouchi, T. Shimizu, T. Oikawa, O. Sakata, H. Uchida, Y. Imai, T. Kiguchi, T. J. Konno, H. Funakubo, Appl. Phys. Lett. **108**, 262904 (2016)
46. S.J. Kim, D. Narayan, J.-G. Lee, J. Mohan, J.S. Lee, J. Lee, H.S. Kim, Y.-C. Byun, A.T. Lucero, C.D. Young, S.R. Summerfelt, T. San, L. Colombo, J. Kim, Appl. Phys. Lett. **111**, 242901 (2017)
47. J.E. Lowther, J.K. Dewhurst, J.M. Leger, J. Haines, Phys. Rev. B **60**, 14485 (1999)
48. M.H. Park, Y.H. Lee, H.J. Kim, Y.J. Kim, T. Moon, K.D. Kim, S.D. Hyun, T. Mikolajick, U. Schroeder, C.S. Hwang, Nanoscale **10**, 716 (2018)
49. M.H. Park, Y.H. Lee, T. Mikolajick, U. Schroeder, C. S. Hwang, Adv. Electron. Mater. **5**, 1800522 (2019)
50. M.H. Park, C.C. Chung, T. Schenk, C. Richter, K. Opsomer, C. Detavernier, C. Adelmann, J.L. Jones, T. Mikolajick, U. Schroeder, Adv. Electron. Mater. **4**, 1800091 (2018)
51. S.-H. Guan, X.-J. Zhang, Z.-P. Liu, J. Am. Chem. Soc. **137**, 8010 (2015)
52. Y.H. Lee, S.D. Hyun, H.J. Kim, J.S. Kim, C. Yoo, T. Moon, K.D. Kim, H.W. Park, Y.B. Lee, B.S. Kim, J. Roh, M.H. Park, C.S. Hwang, Adv. Electron. Mater. **5**, 1800436 (2019)